LETTER

doi:10.1038/nature14105

Impact jetting as the origin of chondrules

Brandon C. Johnson[1], David A. Minton[2], H. J. Melosh[2] & Maria T. Zuber[1]

Chondrules are the millimetre-scale, previously molten, spherules found in most meteorites[1]. Before chondrules formed, large differentiating planetesimals had already accreted[2]. Volatile-rich olivine reveals that chondrules formed in extremely solid-rich environments, more like impact plumes than the solar nebula[3–5]. The unique chondrules in CB chondrites probably formed in a vapour-melt plume produced by a hypervelocity impact[6] with an impact velocity greater than 10 kilometres per second. An acceptable formation model for the overwhelming majority of chondrules, however, has not been established. Here we report that impacts can produce enough chondrules during the first five million years of planetary accretion to explain their observed abundance. Building on a previous study of impact jetting[7], we simulate protoplanetary impacts, finding that material is melted and ejected at high speed when the impact velocity exceeds 2.5 kilometres per second. Using a Monte Carlo accretion code, we estimate the location, timing, sizes, and velocities of chondrule-forming impacts. Ejecta size estimates[8] indicate that jetted melt will form millimetre-scale droplets. Our radiative transfer models show that these droplets experience the expected cooling rates of ten to a thousand kelvin per hour[9,10]. An impact origin for chondrules implies that meteorites are a byproduct of planet formation rather than leftover building material.

Recent work shows that the iSALE hydrocode[11,12] is capable of modelling the extreme process of impact jetting[7]. While previous models focused on impacts between strengthless fluid bodies[7], here we determine the effect that porosity and material strength have on the jetting process (Methods). Using iSALE we simulate vertical impacts of initially fractured dunite impactors of 1%, 10%, and 25% porosity and 10-km diameter on flat targets at impact velocity $v_{imp} = 1$–$6\,km\,s^{-1}$ stepping up by $0.5\,km\,s^{-1}$ (Methods). Later, we scale our results to larger impactor sizes using hydrodynamic similarity[13]. We find that no melted material (Methods) ejected above escape velocity is resolved for impacts with $v_{imp} < 2.5\,km\,s^{-1}$, assuming that v_{imp}/v_{esc} is between 0.5 and 2, where v_{esc} is the escape velocity. During the impact simulation shown in Fig. 1, a total mass of material equivalent to ~1% of the impactor's mass is melted and ejected at higher than escape velocity for an assumed $v_{imp}/v_{esc} = 1$.

As shown in Fig. 1, jetting melts and ejects near-surface material at high velocity. Thermal modelling and palaeomagnetism of chondrites indicate that some differentiated planetesimals had outer shells of undifferentiated material[14]. If this near-surface material is undifferentiated, jetting will produce chondrules with primitive compositions[15]. This is in contrast to other models that rely on splashing during low-velocity ($v_{imp} \approx 10$–$100\,m\,s^{-1}$) collisions between already molten planetesimals[16,17]. It is doubtful that ejection of previously molten and differentiated[2] material would produce chemically unfractionated chondrules[18]. Moreover, collisional splashing creates 'droplets' that are approximately 40 m in diameter (Methods). Previous size estimates[16], which agreed with observed chondrule sizes, neglected the effect of decompression heating[19].

Using the GAME Monte Carlo accretion code[20] we are able to determine where and when chondrule-forming impacts will occur. We model a typical minimum mass solar nebula (MMSN) and a three times more massive nebula (3MMSN), both of which extend from 0.4 astronomical units (AU) to 4 AU (ref. 20). Initially, solid bodies have a main-belt-like size frequency distribution between 100 km and 1,000 km in diameter[21] (Methods). In addition to these bodies, our models include the eccentricity damping effect of nebular gas[20]. As Fig. 2 shows, chondrule-forming impacts occur about 10^3–10^4 yr into the simulation. Assuming that the initial conditions of our model correspond to the time of CAI formation t_{CAI}, this timing of chondrule formation is consistent with the age of the oldest chondrules, $t_{CAI} \pm 0.4$ million years (Myr) (ref. 22).

The target bodies for impacts with $v_{imp} < 2.5\,km\,s^{-1}$ are planetary embryos more massive than the Moon. This explains how impacts,

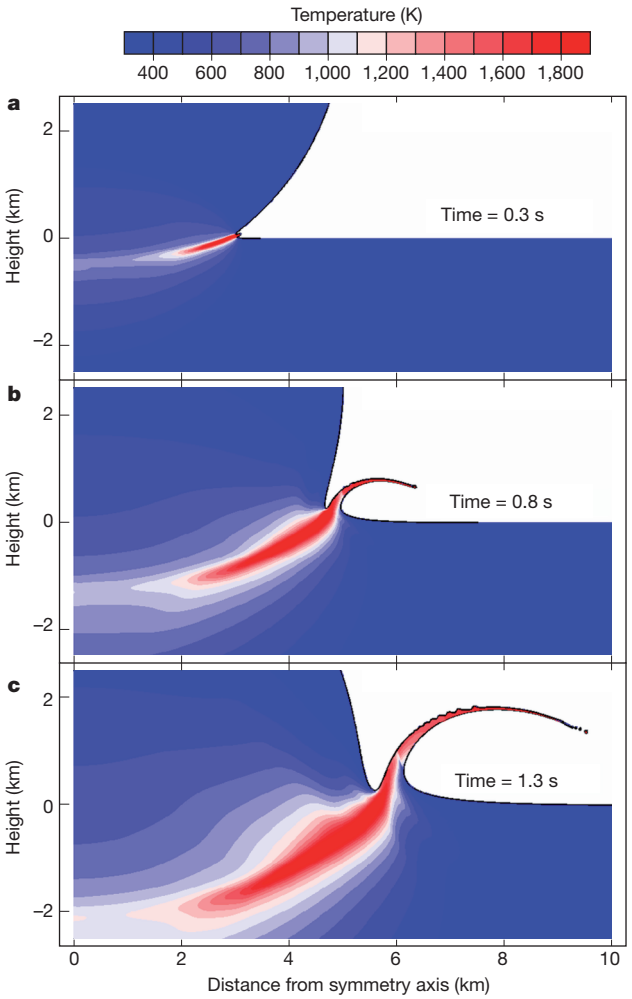

Figure 1 | Jetting of melted material during an accretionary impact. A time series showing a 1% porous projectile 10 km in diameter striking a target at $3\,km\,s^{-1}$. Material is coloured according to its temperature at the time shown. The origin is the collision site. In **a** the jet is just beginning to form, 0.3 s into the impact. Panel **b** shows a well-formed hot jet 0.8 s into the impact. Panel **c** roughly shows the end of jetting, when the projectile penetrates halfway into the target. The fastest ejecta have a velocity of about $6\,km\,s^{-1}$, or twice the impact velocity. The figure was produced using iSALEPlot.

[1]Department of Earth, Atmospheric and Planetary Sciences, Massachusetts Institute of Technology, 77 Massachusetts Avenue, Cambridge, Massachusetts 02139, USA. [2]Department of Earth, Atmospheric, and Planetary Sciences, Purdue University, 550 Stadium Mall Drive, West Lafayette, Indiana 47907, USA.

which eject much more solid material than melted material, can produce chondrule-rich chondrites. The only material that escapes the target bodies is a high-speed mixture of melted surface material (nascent chondrules) and lightly shocked cold proto-matrix (matrix is the material in which chondrules are embedded, and shocking refers to the increase in material temperature and pressure by passage of a shock wave). Most of the lower-speed solid ejecta are retained because of the target bodies' large escape velocity. The ejected chondrules and dust are decelerated to low relative velocities by lingering nebular gas, and preferentially accrete onto smaller planetesimals, which collectively have a larger surface area than more massive bodies[23].

Chondrule formation stopped sometime around 5 Myr after t_{CAI} (refs 1 and 22). In our models, large impacts continue to occur even after 5 Myr. However, chondrules are ejected at velocities above about 2.5 km s^{-1} and will have dynamically excited orbits. Without significant gas present to reduce the eccentricities and inclinations of their orbits, chondrules will break up as they collide with one another or larger bodies at velocities comparable to their ejection velocity of a few kilometres per second. Astronomical observations suggest that the mean lifetime of a primordial protoplanetary disk is about 3 Myr (ref. 24). Melt ejected below escape velocity is bound to the target bodies, which are too large to be disrupted by impacts, and must be dynamically removed from the asteroid belt[25].

The earliest chondrule-forming impacts occur closer to the Sun and the position where chondrule formation occurs moves outward with time (Fig. 2). 5 Myr into accretion, the outermost chondrule-forming impacts occur within 2.2 AU and 3.9 AU, respectively, for the MMSN and 3MMSN models (the main asteroid belt extends from ~2 AU to 3 AU). With masses of 10^{20}–10^{23} kg, the impacting bodies range in size from nearly that of Vesta to larger than the Moon (Fig. 2a). The maximum impact velocity and v_{imp}/v_{esc} increase as time goes on (Extended Data Fig. 1). As v_{imp}/v_{esc} increases, fractionally more unmelted material is ejected at higher than escape velocity. Thus, our model predicts that chondrites formed further away from the Sun should form later and on average be richer in matrix than those that formed closer to the Sun.

Using hydrodynamic scaling and estimates of the melt mass ejected above escape velocity as a function of v_{imp}/v_{esc} for each of our iSALE models (Methods), we estimate the mass of chondrules created by each accretionary impact occurring in our GAME simulation. The 287 chondrule-forming impacts in the MMSN model produce more than 2×10^{22} kg of chondrules while the 4776 chondrule-forming impacts in the 3 MMSN model make over 4×10^{23} kg of chondrules for the 1% porosity case (Fig. 3). Jetted mass is expected to increase significantly for impacts on more realistic curved targets[7,26] and may also increase when oblique impacts are considered[26,27]. The threshold velocity of 2.5 km s^{-1} required to produce chondrules may be an overestimate for the same reasons. A lower threshold velocity would produce more chondrules further out in the disk, as does using a different size distribution for the initial conditions of GAME (Methods). Thus, the estimates shown in Fig. 3 probably represent a minimum approximation for the total mass of chondrules that impacts can produce.

The present asteroid belt has a mass $M_{mb} = 3 \times 10^{21}$ kg and is depleted in mass by a factor of ~1,000 from a MMSN[28]. This corresponds to a numerical depletion factor of 10–100 because most of the mass was contained in large planetary embryos[28]. Chondrules will preferentially accrete onto smaller bodies, which have a larger collective surface area than more massive bodies. Consequently, assuming the main-belt is about one-third chondrules by mass, a successful chondrule formation mechanism must produce ~$3M_{mb}$ to $30M_{mb}$ of chondrules[23]. Although dynamical models indicate that ~10%–30% of the asteroid belt mass may be material originally from 1.5–2 AU (ref. 25), our MMSN model only makes $8M_{mb}$ in total. However, a 3MMSN model makes ~$142M_{mb}$ of chondrules with $11M_{mb}$ being made in the main-belt region (2–3 AU). Therefore, even with reasonable assumptions our lower limit estimates suggest that impacts produce enough chondrules to explain the current chondrule abundance.

The igneous textures that chondrules exhibit imply that they cooled at rates of 10–1,000 K h^{-1} (refs 9 and 10). Using a one-dimensional radiative transfer code, and a geometry that approximates that of jetted material (Methods, Extended Data Fig. 3), we determine the average cooling rates of impact-produced chondrules for a range of impactor sizes (Fig. 4, Methods). Our simulations indicate that jetted material cools at rates of 10–1,000 K h^{-1} for impactors that are hundreds to thousands of kilometres in diameter. These estimates demonstrate that melted droplets jetted during large-scale accretionary impacts will exhibit the observed igneous textures of chondrules.

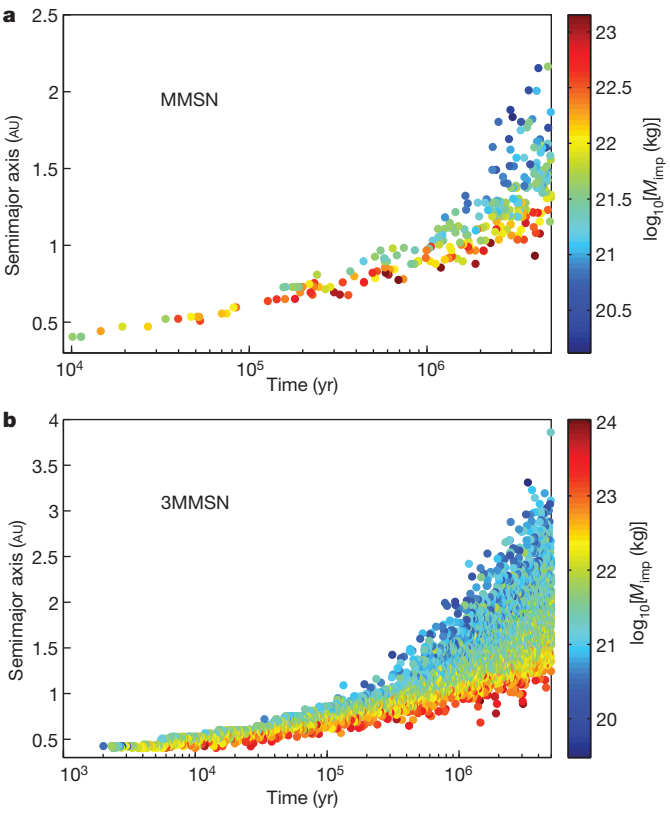

Figure 2 | Timing and location of chondrule-forming impact. Chondrule-forming impacts with velocities above 2.5 km s^{-1} for the MMSN model (**a**) and the 3MMSN model (**b**). The points are coloured according to the logarithm of the mass of the impacting body marked on the corresponding colour bar.

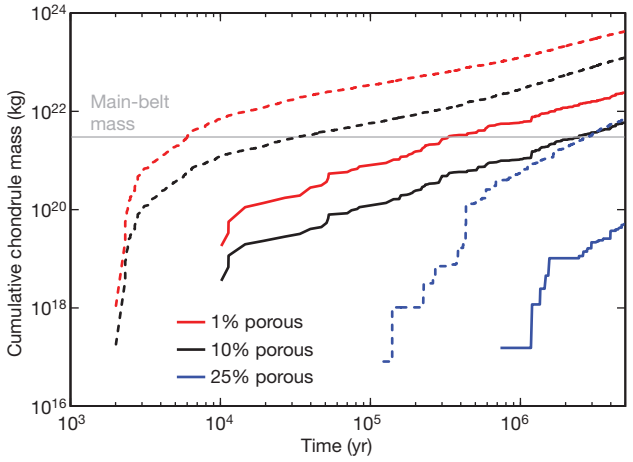

Figure 3 | The cumulative mass of chondrules created by accretionary impacts. The red, black and blue curves show model results for 1%, 10%, and 25% initial porosities. The solid curves correspond to the MMSN model and the dashed curves correspond to the 3MMSN model. The grey line acts as a guide to the eye, showing the mass of the main asteroid belt, at 3×10^{21} kg.

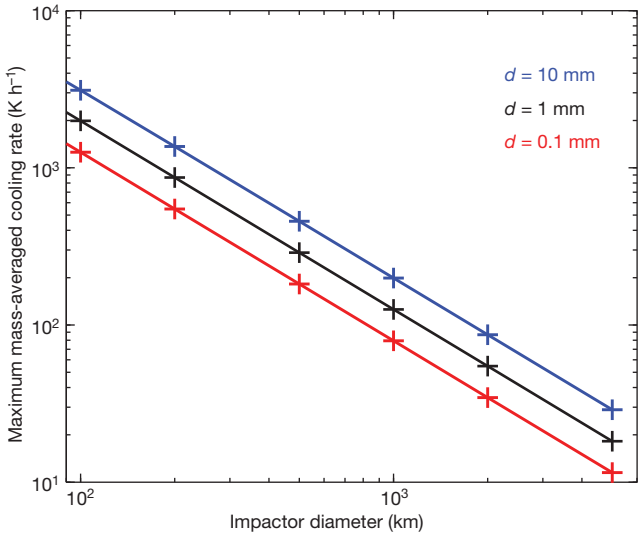

Figure 4 | Chondrule cooling rates as a function of impactor size. The coloured lines represent different assumed droplet diameters d within the jet, as indicated. The crosses represent actual model runs.

The chondrules found within a given chondrite type exhibit significant variations in composition[1,29]. Turbulence within the jet and chondrule–chondrule collisions may mix material on scales comparable to the thickness of the jet. However, the jet is composed of a mixture of target and projectile material and the ratio of target-to-projectile material changes with time[7]. If near surface material from the target and projectile have significantly different compositions, the chondrules produced by the impact will be chemically diverse. Expected spatial variations in chondrule number density could also contribute to the observed compositional diversity[30].

An important aspect of our model is that, although chondrules accumulate to form chondrites on small bodies, the chondrules themselves are formed by impacts on much larger bodies. Because of this, only a small fraction of the mass of the terrestrial planets is processed into chondrules. Thus, we argue that chondrules are not the direct building blocks of the planets, but merely a byproduct of their accretion.

Online Content Methods, along with any additional Extended Data display items and Source Data, are available in the online version of the paper; references unique to these sections appear only in the online paper.

Received 16 July; accepted 20 November 2014.

1. Scott, E. R. D. Chondrites and the protoplanetary disk. *Annu. Rev. Earth Planet. Sci.* **35,** 577–620 (2007).
2. Kruijer, T. S. *et al.* Protracted core formation and rapid accretion of protoplanets. *Science* **344,** 1150–1154 (2014).
3. Fedkin, A. V. & Grossman, L. Vapor saturation of sodium: key to unlocking the origin of chondrules. *Geochim. Cosmochim. Acta* **112,** 226–250 (2013).
4. Alexander, C. M. O. & Ebel, D. S. Questions, questions: Can the contradictions between the petrologic, isotopic, thermodynamic, and astrophysical constraints on chondrule formation be resolved? *Meteorit. Planet. Sci.* **47,** 1157–1175 (2012).
5. Alexander, C. M. O., Grossman, J. N., Ebel, D. S. & Ciesla, F. J. The formation conditions of chondrules and chondrites. *Science* **320,** 1617–1619 (2008).
6. Krot, A. N., Amelin, Y., Cassen, P. & Meibom, A. Young chondrules in CB chondrites from a giant impact in the early Solar System. *Nature* **436,** 989–992 (2005).
7. Johnson, B. C., Bowling, T. J. & Melosh, H. J. Jetting during vertical impacts of spherical projectiles. *Icarus* **238,** 13–22 (2014).
8. Johnson, B. C. & Melosh, H. J. Formation of melt droplets, melt fragments, and accretionary impact lapilli during a hypervelocity impact. *Icarus* **228,** 347–363 (2014).
9. Lofgren, G. & Russell, W. J. Dynamic crystallization of chondrule melts of porphyritic and radial pyroxene composition. *Geochim. Cosmochim. Acta* **50,** 1715–1726 (1986).
10. Desch, S. J., Morris, M. A., Connolly, H. C. & Boss, A. P. The importance of experiments: constraints on chondrule formation models. *Meteorit. Planet. Sci.* **47,** 1139–1156 (2012).
11. Collins, G. S., Melosh, H. J. & Ivanov, B. A. Modeling damage and deformation in impact simulations. *Meteorit. Planet. Sci.* **39,** 217–231 (2004).
12. Wünnemann, K., Collins, G. S. & Melosh, H. J. A strain-based porosity model for use in hydrocode simulations of impacts and implications for transient crater growth in porous targets. *Icarus* **180,** 514–527 (2006).
13. Melosh, H. J. *Impact Cratering: a Geologic Process* (Oxford Univ. Press, 1989).
14. Weiss, B. P. & Elkins-Tanton, L. T. Differentiated planetesimals and the parent bodies of chondrites. *Annu. Rev. Earth Planet. Sci.* **41,** 529–560 (2013).
15. Bland, P. A. *et al.* Volatile fractionation in the early solar system and chondrule/matrix complementarity. *Proc. Natl Acad. Sci. USA* **102,** 13755–13760 (2005).
16. Asphaug, E., Jutzi, M. & Movshovitz, N. Chondrule formation during planetesimal accretion. *Earth Planet. Sci. Lett.* **308,** 369–379 (2011).
17. Sanders, I. S. & Scott, E. R. D. The origin of chondrules and chondrites: debris from low-velocity impacts between molten planetesimals? *Meteorit. Planet. Sci.* **47,** 2170–2192 (2012).
18. Taylor, G. J., Scott, E. R. D. & Keil, K. Cosmic setting for chondrule formation. In *LPI Conf. on 'Chondrules and their Origins'* **493,** abstract 58, http://adsabs.harvard.edu/abs/1983chto.conf..262T (1982).
19. Mastin, L. G. & Ghiorso, M. S. Adiabatic temperature changes of magma–gas mixtures during ascent and eruption. *Contrib. Mineral. Petrol.* **141,** 307–321 (2001).
20. Minton, D. A. & Levison, H. F. Planetesimal-driven migration of terrestrial planet embryos. *Icarus* **232,** 118–132 (2014).
21. Morbidelli, A., Bottke, W. F., Nesvorný, D. & Levison, H. F. Asteroids were born big. *Icarus* **204,** 558–573 (2009).
22. Connelly, J. N. *et al.* The absolute chronology and thermal processing of solids in the solar protoplanetary disk. *Science* **338,** 651–655 (2012).
23. Hood, L. L. & Weidenschilling, S. J. The planetesimal bow shock model for chondrule formation: a more quantitative assessment of the standard (fixed Jupiter) case. *Meteorit. Planet. Sci.* **47,** 1715–1727 (2012).
24. Evans, N. J. I. *et al.* The Spitzer c2d legacy results: star-formation rates and efficiencies; evolution and lifetimes. *Astrophys. J.* **181** (Suppl.), 321–350 (2009).
25. O'Brien, D. P., Morbidelli, A. & Bottke, W. F. The primordial excitation and clearing of the asteroid belt—revisited. *Icarus* **191,** 434–452 (2007).
26. Melosh, H. J. & Sonett, C. P. When worlds collide—jetted vapor plumes and the Moon's origin. In *LPI Conf. on 'Origin of the Moon'* **1,** 621–642, http://adsabs.harvard.edu/abs/1986ormo.conf.621M (1986).
27. Vickery, A. M. The theory of jetting: application to the origin of tektites. *Icarus* **105,** 441–453 (1993).
28. Weidenschilling, S. J. Initial sizes of planetesimals and accretion of the asteroids. *Icarus* **214,** 671–684 (2011).
29. Hezel, D. C. & Palme, H. The conditions of chondrule formation, Part I: Closed system. *Geochim. Cosmochim. Acta* **71,** 4092–4107 (2007).
30. Cuzzi, J. N. & Alexander, C. M. O. Chondrule formation in particle-rich nebular regions at least hundreds of kilometres across. *Nature* **441,** 483–485 (2006).

Acknowledgements We thank I. Sanders for his review, which improved the manuscript. We gratefully acknowledge the developers of iSALE (www.isale-code.de/projects/iSALE), especially G. Collins, K. Wünnemann, D. Elbeshausen and B. Ivanov. This research was supported by NASA grant number PGG NNX10AU88G.

Author Contributions While working on calculating the cooling rates of impact-produced chondrules with H.J.M., B.C.J. conceived the idea that chondrules could form by jetting during low-velocity accretionary impacts. D.A.M. produced the Monte Carlo accretion code results. B.C.J. produced the hydrocode and radiative transfer code results. All authors contributed to preparation of the manuscript and the conclusions presented in this work.

Author Information Reprints and permissions information is available at www.nature.com/reprints. The authors declare no competing financial interests. Readers are welcome to comment on the online version of the paper. Correspondence and requests for materials should be addressed to B.C.J. (brcjohns@mit.edu).

METHODS

Droplet sizes jetting model. Assuming that a model for melt droplet formation in ejecta curtains[8] can be extended to droplet formation in jetted material, we calculate the size of chondrules with ejection velocities equal to the impact velocity (Extended Data Fig. 2). However, jetting ejects material at velocities above the impact velocity and higher ejection velocities yield smaller droplets. Consequently, the droplet sizes in Extended Data Fig. 2 are the maximum size of droplets produced by jetting. For chondrule-forming impacts with impact velocities of 2.5–5.5 km s^{-1} and impactor sizes of 100–1,000 km, jetted material will create millimetre-scale droplets consistent with the observed size of chondrules (Extended Data Fig. 2).

In terrestrial impact ejecta deposits, larger, centimetre-scale tektites (or melt fragments) are found along with millimetre-scale melt droplet spherules[8], whereas chondrules are all roughly the same size[18]. For terrestrial impacts, the initial dynamic fragmentation[31] of melt forms centimetre-scale droplets[8]. Upon release from high pressure, more highly shocked material or more-volatile-rich material separates into vapour and liquid. Acceleration of this vapour–liquid mix produces a differential velocity between droplets and the surrounding vapour and the balance of inertial forces and surface tension determines the droplet size[8]. The droplets formed in this accelerated two-phase mixture are roughly millimetre-scale for terrestrial impact conditions. The volatile-rich nature of chondrule precursor material may explain the apparent lack of tektite-like chondrules. Essentially, if any silicates are shock-melted there will be enough vaporized volatiles present that the material will be best described by a vapour–liquid mixture.

Droplet sizes splashing model. Droplet size estimates from the splashing model for chondrule formation[16] assume that the pv component of specific enthalpy $h = q + pv$ (where q is specific internal energy, p is pressure, and v is specific volume) is converted to surface energy of droplets with nearly perfect efficiency. Cavitation and droplet formation does not occur until $p < 0$ and when $p = 0$ the pv component of enthalpy is also zero. Thus, when ex-solution of gases is ignored, isenthalpic release from pressure p causes decompression heating (that is, the pv part of enthalpy is converted to internal energy q)[19]. Even for a magma releasing to zero pressure from 200 MPa the associated temperature change is only 50 K (ref. 19). Because there is no pv component of enthalpy at the time of fragmentation, the assumption that all enthalpy is converted to surface energy is unphysical. The actual size of the 'droplets' is then determined by the balance of inertial forces and tensional forces[31]. For typical strain rates of $\dot{\epsilon} \approx 1\ \mathrm{h}^{-1}$ (ref. 16), surface tension of $\sigma = 0.3\ \mathrm{N\ m}^{-1}$, density $\rho = 3{,}000\ \mathrm{kg\ m}^{-3}$ splashing will create 'droplets' with diameter $d = (40\sigma/\rho\dot{\epsilon}^2)^{\frac{1}{3}} \approx 40$ m (refs 8 and 31).

Hydrocode modelling. Extended Data Table 1 describes the input parameters used in our iSALE models. The number of equations of state that accurately represent geologic materials under the extreme conditions occurring during impacts is small. Here we use equations of state for dunite[32], produced by the ANEOS program[33], to approximate the bulk properties of the impactors and target bodies during accretion. We use dunite strength, thermal softening and porous compaction parameters from refs 34–36 and references therein.

During the jetting process, material is first shocked and then adiabatically compressed[7]. Consequently, we cannot calculate the amount of material melted during an impact using the peak pressure. Instead, we use the post-release temperature to estimate the amount of melt. We consider any mass that releases to temperatures above 1,373 K to be potentially chondrule-forming mass. We use the solidus temperature because ANEOS does not account for the latent heat of fusion. Hence, temperatures above the solidus are exaggerated and cannot be trusted[37]. Additionally, ANEOS in its current form tends to underpredict the entropy of geologic material shocked to a given pressure[38,39]. This means that ANEOS tends to underestimate the degree of melting and the temperatures after release.

For a given impact velocity the total mass of melt ejected above some ejection velocity v_{ej} is calculated by summing the mass of Lagrangian tracers with $v > v_{ej}$ that also release to temperatures above 1,373 K. For a more detailed description of Lagrangian tracers and how ejection velocities are determined see ref. 8. For each impactor and target porosity, we created lookup tables for the melt mass ejected at greater than escape velocity as a function of impact velocity and escape velocity. These tables cover $v_{imp}/v_{esc} = 0.5$–2 stepping by 0.1, and $v_{imp} = 2.5$–6 km s^{-1} stepping by 0.5 km s^{-1}. Using these tables and hydrodynamic similarity[13], we estimate the amount of melt created by all of the impacts occurring in the GAME model. For impacts with v_{imp}/v_{esc} and/or v_{imp} falling between the data points from our iSALE models, we use bi-linear interpolation to estimate the fraction of impactor mass that is melted and ejected at higher than escape velocity.

To check the assumption of hydrodynamic similarity we ran a model with an impactor of 1,000 km diameter and found that the amount of melted and jetted material, normalized by impactor mass, did not change. We also made a run with the target and impactor initially having intact rock strength. This run was only minimally different, less than 1%, from the results using an originally damaged impactor and target. Thus, we conclude that material strength has a very limited effect on jetting efficiency at least for impact velocities above 2.5 km s^{-1}. However, as porosity increases, the overall jetting efficiency decreases significantly. This is consistent with jetting being less efficient in more compressible materials[7].

Code availability. At present, iSALE is not fully open source. It is distributed on a case-by-case basis to academic users in the impact community, strictly for non-commercial use. Scientists interested in using or developing iSALE should see http://www.isale-code.de/redmine/projects/isale/wiki/Terms_of_use for a description of application requirements. The one-dimensional radiative transfer code used here is available on request from B. Johnson (brcjohns@mit.edu). GAME is available upon request from D. Minton (daminton@purdue.edu).

Monte Carlo accretion. The minimum mass solar nebula (MMSN) describes a disk that is just massive enough to create the observed planets. The MMSN implicitly assumes that no mass is lost from the solar nebula during the planet formation process. More massive solar nebulae are often considered by dynamical modellers[20]. In the 3MMSN model a small fraction of impacts have $v_{imp} > 6$ km s^{-1} and $v_{imp}/v_{esc} > 2$. In our chondrule mass calculation, we do not include these impacts. This omission changes our mass estimate by only a few per cent, an error that is much smaller than the uncertainties inherent to our calculation.

We modelled disks with a main-belt-like size frequency distribution between 100 km and 1,000 km (ref. 21). This size frequency distribution (SFD) was proposed[21] because it can produce embryos of larger than the Moon's mass before the protoplanetary disk dissipates (~3 Myr). The early formation of embryos is required to explain the mass depletion and dynamical state of the main belt[25]. Other models show that an initially monodisperse population of planetesimals of 0.1 km diameter can create larger-than-lunar mass embryos and the observed size frequency of main-belt asteroids in just 10^5 yr (ref. 28). Because GAME tracks the accretion history of each object in the model, starting with planetismals of 0.1 km diameter is computationally unfeasible. However, we did model disks with a distribution of bodies generated from a Gaussian distribution centred at 100 km in diameter with a 50-km standard deviation (truncated at 0 km).

The MMSN model with a Gaussian SFD produced 0.86, 0.86, and 1.9 times the mass of chondrules made in the MMSN model with a main-belt like SFD, for 1%, 10%, and 25% porous cases, respectively. The 3MMSN model with a Gaussian SFD produced 0.52, 0.45, and 0.22 times the mass of chondrules made in the 3MMSN model with a main-belt-like SFD, for 1%, 10%, and 25% porous cases, respectively. We also found this Gaussian SFD produced chondrules somewhat closer to the Sun. For the MMSN models, by 5 Myr the Gaussian SFD produced chondrules at 1.6 AU from the Sun, whereas the main-belt-like SFD produced chondrules at 2.2 AU. For the 3MMSN models, by 5 Myr the Gaussian SFD produced chondrules at 2.4 AU, whereas the main-belt-like SFD produced chondrules at 3.9 AU.

Radiative transfer and cooling rates. We find the geometry of a spherically expanding plume, as used by ref. 40, is unrealistic for jetted melt. To estimate the cooling rates of impact-produced melt droplets, we model the ejected material as an infinite sheet with a density that decreases with time. We assume this geometry so we can use a one-dimensional radiative transfer code to determine the cooling rates. Our radiative transfer code uses the diffusion approximation[41]. We benchmarked the code using the non-equilibrium Marshak diffusion problem[42]. Extended Data Fig. 3 schematically shows our assumed geometry, where

$$R_{in}(t) = R_{in}(t_0) + v_{in}t$$

$$R_{out}(t) = R_{out}(t_0) + v_{out}t$$

We consider the case where $v_{in} = v_{imp} = 3$ km s^{-1} and $v_{out} = 3.5$ km s^{-1}. At 2.5 s into the impact of a 10-km-diameter projectile, $R_{in} = 8.8$ km and $R_{out} = 9.5$ km. This region has an average density of $\rho_{jet} = 800\ \mathrm{kg\ m}^{-3}$ and an average thickness of $h = 215$ m. The 7×10^{12} kg of material represents 48% of the total melt mass ejected with velocities above 3 km s^{-1}. This is the result of lower-velocity material dominating the mass of the jet[7]. When considering larger impactor sizes we use hydrodynamic scaling to produce different initial conditions.

We focus on the mass-averaged cooling rate of this material as an estimate for the average cooling rate of chondrules created by jetting. If we were to consider faster parts of the plume, we would expect higher cooling rates; slower ejecta would have lower cooling rates.

We assume the heat capacity of the droplets to be 1,000 J kg^{-1} K^{-1} and the bulk density of the droplets is $\rho_{drop} = 3{,}000\ \mathrm{kg\ m}^{-3}$. The droplets are assumed to be blackbodies and thus have a collective opacity of $\kappa = 3\phi/4r_{drop}$, where ϕ is the fraction of the volume occupied by the droplets and r_{drop} is the radius of the of the melt droplets. For simplicity, we neglect the opacity of any vapour that may be present, that is, impact-produced vapour or gas in the solar nebula. We assume that the droplets start out with temperatures of 2,000 K. We also set the constant temperature boundary condition to 300 K.

The opacity is updated using the volume calculated at each time step:

$$V(t) = \pi\left(R_{\text{out}}^2 - R_{\text{in}}^2\right) \mathrm{d}h$$

where $\mathrm{d}h = h/800$ is the thickness of one of 400 equal-sized computational cells. Note that for the reflective boundary condition and symmetry of the problem we model only half of the thickness of the jet. Then the volume fraction occupied by molten droplets is:

$$\phi = \frac{M_0}{\rho_{\text{drop}} V}$$

where

$$M_0 = \rho_{\text{jet}} V(t_0)$$

In our approximation of the geometry of a jet, radiation escapes only from the free surface of the jet. We find for impactors 100–1,000 km in size that the cooling of the jet takes hours to days (Fig. 4). The fastest part of the jet moves a few kilometres per second faster than the parts that only just escape the target body. Thus, the jet has a horizontal extent of 10^4–10^5 km on the timescale of cooling (estimated by multiplying a few kilometres per second by an hour to a day). The distance over which radiation must diffuse is much larger than the thickness scale, which is 2–20 km for impactors that are 100–1,000 km in diameter. Additionally, the free surface is much colder (here assumed to be 300 K) when compared to the temperature of adjacent material along the jet. Thus, our assumption that radiative transfer along the jet is negligible is quite reasonable.

Extended Data Fig. 4 shows the results of our radiative transfer code, assuming a droplet diameter of 1 mm and an impactor diameter of 1,000 km. Extended Data Fig. 4 shows that the maximum mass-averaged cooling rate, which is plotted in Fig. 4, occurs when the mass-averaged temperature is ~1,400 K. The plots also show that the outer part of the jet cools at about ten times the rate of the inner part of the jet. The outer part of the jet is not to be confused with the faster-moving part of the jet (see Extended Data Fig. 3), although faster-moving parts of the jet probably have higher cooling rates too.

Dust enrichment and chondrule–chondrule collisions. Turbulent mixing of nebular gas and jetted material lead to chondrule–chondrule collisions. In the jet the turbulent velocity is approximately a few per cent of the flow velocity, which is the product of the jet thickness and local velocity gradient[8]. This velocity is independent of impactor size and our iSALE models indicate that the turbulent velocity of the jet is $v_{\text{turb}} \approx 5\ \text{m s}^{-1}$. However, the turbulent velocity may be a few per cent of the ejection velocity, $v_{\text{turb}} \approx 100\ \text{m s}^{-1}$, if turbulence created at the jet–nebula interface is dominant. The relative velocities of inertial particles in turbulent two-fluid flow is[42]:

$$v_{\text{rel}} = v_{\text{turb}}\left(1 + 1.5\tau_{\text{p}}\frac{v_{\text{turb}}}{l_{\text{turb}}}\right)^{-1/2}$$

where l_{turb} is the turbulent length scale taken to be approximately equal to the jet thickness of 2.2–22 km for impactor diameters of 100–1,000 km. In the midplane at around 3 AU, $\tau_{\text{p}} = 4.9 \times 10^3$ s for a 1-mm-diameter particle, with longer times occurring outside the midplane[43]. This equation is valid for inertial or heavy particles that have $\tau_{\text{p}} \geq l_{\text{turb}}/v_{\text{turb}}$ and when the collisional mean free path is larger than the correlation length[44]. In a turbulent flow, the correlation of velocity along a line connecting two points separated by λ is[42]:

$$f = \max\left(0,\ 1 - \frac{0.9\epsilon^{\frac{2}{3}}\lambda^{\frac{2}{3}}}{v_{\text{turb}}^2}\right)$$

where dissipation rate $\epsilon \approx v_{\text{turb}}^3/l_{\text{turb}}$. When $f = 0$ the velocities are uncorrelated; $f = 1$ means that the velocities at the two points are identical. The minimum value of λ that yields $f = 1$ is the correlation length. We find that at early times the collisional mean free path λ is much smaller than the correlation length. We therefore introduce the following term to account for particles having initially partially correlated velocities:

$$v_{\text{rel}} = v_{\text{turb}}\left(1 + 1.5\tau_{\text{p}}\frac{v_{\text{turb}}}{l_{\text{turb}}}\right)^{-\frac{1}{2}}(1 - f)$$

Assuming a collision efficiency of unity, the average number of collisions a single chondrule experiences per unit time is[42]:

$$N \approx 4\pi^{\frac{1}{2}} d^2 v_{\text{rel}} n_{\text{c}}$$

so that the mean free path $\lambda = \left(4\pi^{\frac{1}{2}} d^2 n_{\text{c}}\right)^{-1}$. Extended Data Fig. 4 shows the results for number density, relative velocity, rate of collisions and cumulative number of collisions calculated at one-second intervals and using the bulk density coming from the radiative transfer sections. We note that the turbulent velocity is assumed to be constant, although it probably decays with time.

While the drops are still above their solidus, the collision velocities shown in Extended Data Fig. 4b are low and could result in coalescence or bouncing[43]. As time goes on the relative velocities increase, but partially molten, cooling chondrules can survive impacts at velocities up to 100 m s^{-1} (ref. 43). Although our simple calculations show that individual chondrules may experience many collisions (Extended Data Fig. 4c, d), it is unknown what fraction of chondrule collisions will result in the formation of compound chondrules, and the fraction of compound chondrules provides only a minimum estimate of the chondrule concentrations[4,45].

Because we do not include nebular gas in our hydrocode models, the pressure in the jet drops below typical nebular pressures of ~0.01–100 Pa (ref. 3). However, even at background nebula pressures the dust enrichment of the jetted material is enough to explain the volatile content of chondrule olivine. If chondrules formed at typical nebular pressures, dust enrichments greater than 10^6 (where dust enrichment is the solid-to-vapour ratio relative to a system of solar composition[3–5]) are needed to explain the volatile content of chondrule olivine[3–5]. For 1-mm-diameter chondrules with densities of 3,000 kg m^{-3} this corresponds to number densities higher than 10^3–10^4 m^{-3} depending on the total pressure[4]. For the geometry of the jet described in the radiative transfer section and for a 100-km-diameter impactor, the number density will remain above 10^4 m^{-3} until 1.2 h after ejection and drops below 10^3 m^{-3} after 3.9 h (Extended Data Fig. 4a). This time scales linearly with impactor size, meaning that the bulk density of material ejected by a 1,000-km-diameter body remains above 10^4 m^{-3} for about 12 h and above 10^3 m^{-3} for 39 h. A comparison of Extended Data Fig. 4 and Fig. 4 shows that this is more than enough time for chondrules to cool below the solidus at ~1,400 K. Our model also predicts that chondrules that experience higher cooling rates (Extended Data Figs 4 and 5) will cool to the solidus at higher dust enrichments than those made by the same impact with lower cooling rates.

Both dust enrichment and total vapour pressure are important for determining the volatile content of chondrule olivine[3]. To obtain more robust estimates of the time history of dust enrichment, the rate of chondrule–chondrule collisions, and the total vapour pressure, the dynamic interaction of jetted material with nebular gas is required. This requires a two-fluid hydrodynamic code that can accurately model the interactions of particles and gas.

31. Benz, W., Cameron, A. & Melosh, H. J. The origin of the Moon and the single-impact hypothesis III. *Icarus* **81,** 113–131 (1989).
32. Thompson, S. L. & Lauson, H. S. Improvement in the Chart D Radiation-Hydrodynamic Code. III. Revised analytic equations of state. *Sandia Report* SC-RR-71 0174 (1984).
33. Grady, D. E. Local inertial effects in dynamic fragmentation. *J. Appl. Phys.* **53,** 322 (1982).
34. Potter, R. W. K., Collins, G. S., Kiefer, W. S., McGovern, P. J. & Kring, D. A. Constraining the size of the South Pole-Aitken basin impact. *Icarus* **220,** 730–743 (2012).
35. Davison, T. M., Collins, G. S. & Ciesla, F. J. Numerical modelling of heating in porous planetesimal collisions. *Icarus* **208,** 468–481 (2010).
36. Bowling, T. J. *et al.* Antipodal terrains created by the Rheasilvia basin forming impact on asteroid 4 Vesta. *J. Geophys. Res. Planets* (2013).
37. Collins, G. S. & Melosh, H. J. Improvements to ANEOS for multiple phase transitions. *Lunar Planet. Sci. Conf.* **2664** (2014).
38. Kraus, R. G. *et al.* Shock vaporization of silica and the thermodynamics of planetary impact events. *J. Geophys. Res.* **117,** E09009 (2012).
39. Kurosawa, K. *et al.* Shock-induced silicate vaporization: the role of electrons. *J. Geophys. Res.* **117,** E04007 (2012).
40. Johnson, B. C., Minton, D. A. & Melosh, H. J. The impact origin of chondrules. *Lunar Planet. Sci. Conf.* **1471** (2014).
41. Bingjing, S. & Olson, G. L. Benchmark results for the non-equilibrium Marshak diffusion problem. *J. Quant. Spectrosc. Radiat. Transf.* **56,** 337–351 (1996).
42. Abrahamson, J. Collision rates of small particles in a vigorously turbulent fluid. *Chem. Eng. Sci.* **30,** 1371–1379 (1975).
43. Weidenschilling, S. J. Particles in the nebular midplane: collective effects and relative velocities. *Meteorit. Planet. Sci.* **45,** 276–288 (2010).
44. Ormel, C. W. & Cuzzi, J. N. Closed-form expressions for particle relative velocities induced by turbulence. *Astron. Astrophys.* **466,** 413–420 (2007).
45. Ciesla, F. J. Chondrule collisions in shock waves. *Meteorit. Planet. Sci.* **41,** 1347–1359 (2006).
46. Wünnemann, K., Collins, G. S. & Osinski, G. R. Numerical modelling of impact melt production in porous rocks. *Earth Planet. Sci. Lett.* **269,** 530–539 (2008).
47. Collins, G. S., Melosh, H. J. & Wünnemann, K. Improvements to the ε-α porous compaction model for simulating impacts into high-porosity solar system objects. *Int. J. Impact Eng.* **38,** 434–439 (2011).

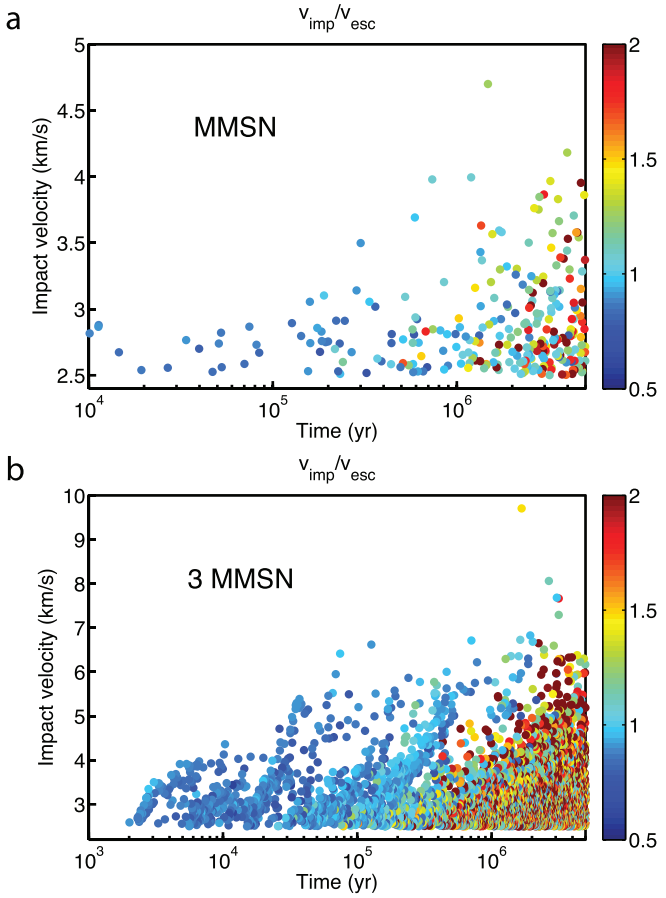

Extended Data Figure 1 | Timing and velocity of chondrule-forming impact. Chondrule-forming impacts with velocities above 2.5 km s^{-1} for the MMSN model (**a**) and the 3MMSN model (**b**). The points are coloured according to v_{imp}/v_{esc} (shown on the colour scale). Note that v_{imp}/v_{esc} may be less than one because v_{esc} is considered to be the escape velocity after the target and impactor have combined to form a more massive body.

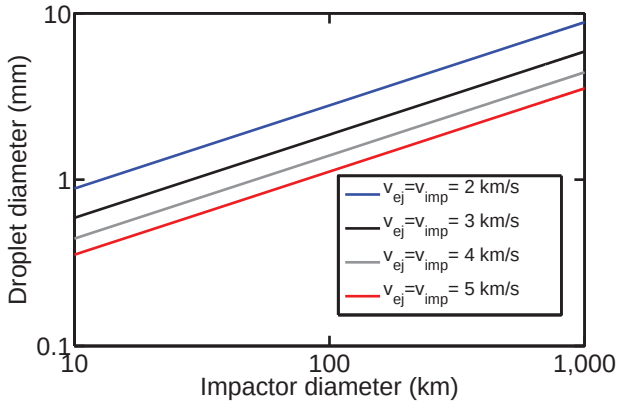

Extended Data Figure 2 | Maximum size of droplets created by jetting. The different lines represent different impact velocities, as indicated.

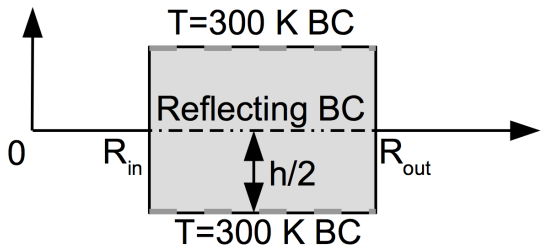

Extended Data Figure 3 | Schematic showing the geometry of our radiative transfer models. The horizontal axis shows radial distance from the point of impact. The vertical axis marks the thickness of the jet. We model a portion of the jet as an annulus that moves outward radially. The width of this annulus also grows with time. BC, boundary condition; *h*, the thickness of the jet.

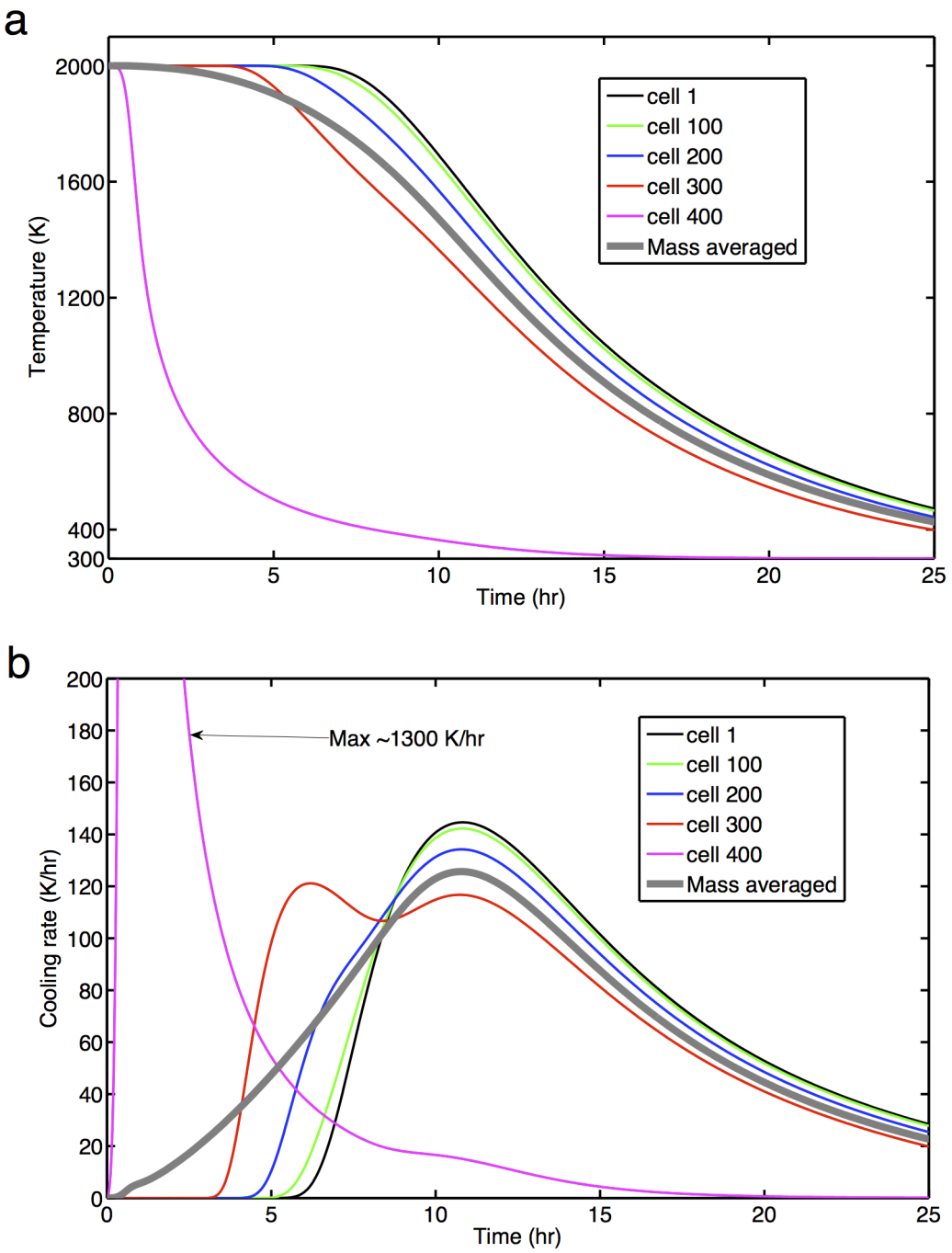

Extended Data Figure 4 | Temperature time history for a jet consisting of 1-mm-diameter droplets created by a 1,000-km-diameter impactor. The different coloured curves represent different computational cells, as indicated, where cell 1 is the innermost cell, which has a reflective boundary condition on one side, and cell 400 is the outermost cell, which radiates into a background at 300 K. The thick grey curve is the mass-averaged temperature, which we use as proxy for the average temperature of material in the plume. Panel **a** shows the temperature as a function of time, while **b** shows the cooling rate as a function of time.

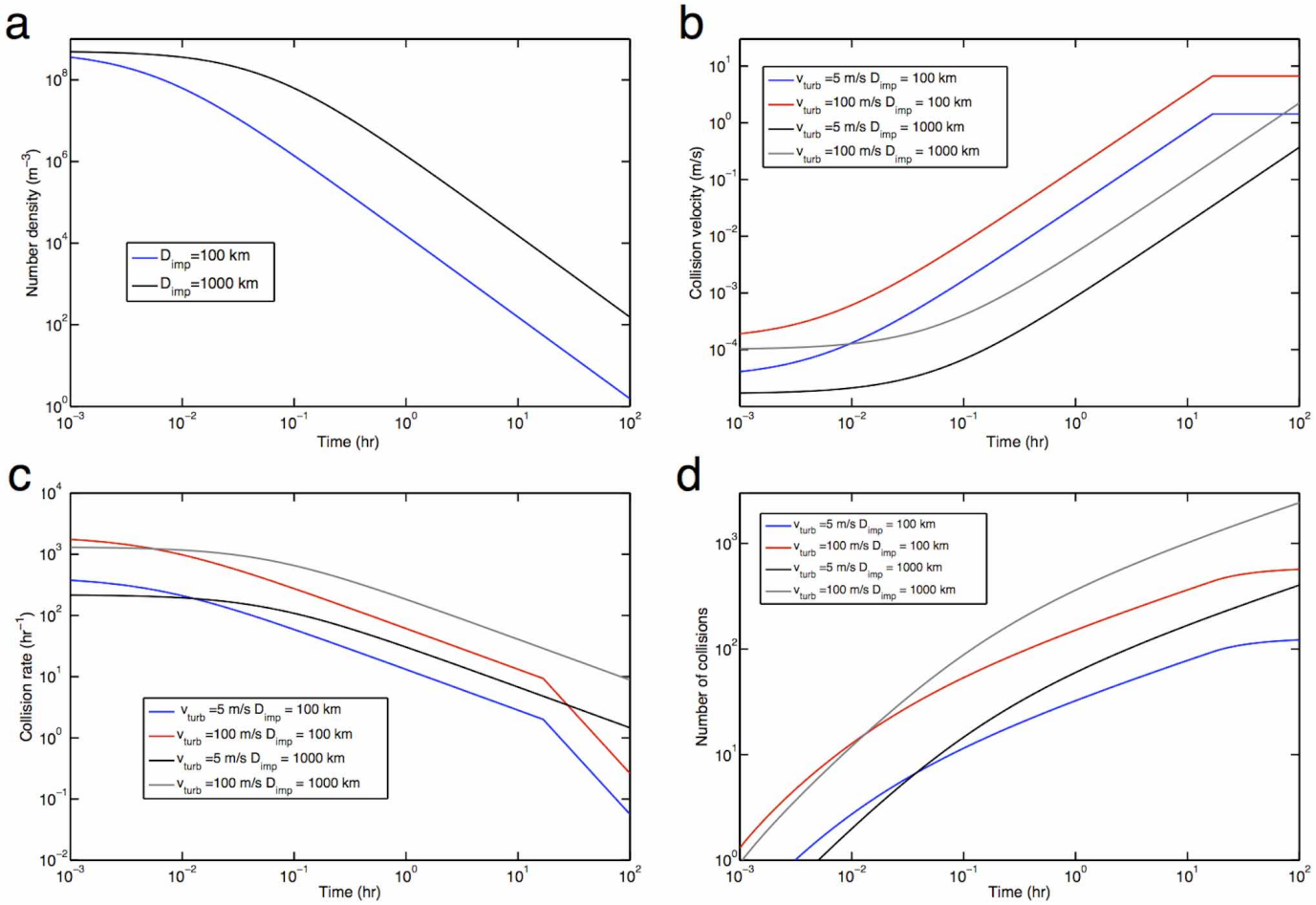

Extended Data Figure 5 | Chondrule density and collision rates. **a**, The number density of chondrules is plotted as a function of time for 100-km-diameter and 1,000-km-diameter impactors. **b**, Relative collision velocity plotted as a function of time. **c**, Rate of collisions a single chondrule experiences plotted as a function of time. **d**, Cumulative number of impacts a chondrule experiences plotted as a function of time.

Extended Data Table 1 | iSALE input parameters

Description	Input
Equation of state	ANEOS dunite[a]
Melting temperature[b]	1373 K
Thermal softening parameter[b]	1.1
Simon A parameter[b]	1520 MPa
Simon B parameter[b]	4.05
Poisson's ratio ν	0.25
Frictional coefficient (damaged) μ[c]	0.63
Frictional coefficient (undamaged) μ[c]	1.58
Strength at infinite pressure Y_m[c]	3.26 GPa
Cohesion (damaged) Y_0[c]	10 kPa
Cohesion (undamaged) Y_0[c]	5.07 MPa
Strain at which porous compaction begins ε_e[d]	0.01
Rate of porous compaction κ[d]	0.98
Size of high resolution cell	12.5 m
Number of high resolution cells horizontal direction	1500
Number of high resolution cells vertical direction	1600
Target and projectile temperature	300 K

[a] See ref. 31.
[b] See ref. 46 and references therein for a description of Simon parameters, the thermal softening parameter, and their implementation in iSALE.
[c] See ref. 11 and references therein for a description of strength model parameters and their implementation in iSALE.
[d] See refs 12 and 47 for a description of the porous compaction model parameters and their implementation in iSALE.